CHALMERS
UNIVERSITY OF TECHNOLOGY

In-situ Formation of Calcium Manganite in Chemical-looping Combustion

Master's thesis in Sustainable energy systems

Elias Landquist

DEPARTMENT of Environmental and Energy Sciences
Division of Energy Technology

CHALMERS UNIVERSITY OF TECHNOLOGY
Gothenburg, Sweden 2026
www.chalmers.se

Master's thesis 2026

In-situ Formation of Calcium Manganite in Chemical-looping Combustion

Elias Landquist

CHALMERS
UNIVERSITY OF TECHNOLOGY

Department of Environmental and Energy Sciences
Division of Energy Technology
CHALMERS UNIVERSITY OF TECHNOLOGY
Göteborg, Sweden 2026

In-situ formation of calcium manganite in chemical-looping combustion

Master’s thesis 2026

Department of Environmental and Energy Sciences
Division of Energy Technology
Chalmers University of Technology
SE-412 96 Göteborg
Sweden
Telephone + 46 31-772 1000

Printed by Chalmers Reproservice
Göteborg, Sweden 2026

In-situ formation of calcium manganite in chemical-looping combustion

Elias Landquist

Department of Environmental and Energy Sciences

Division of Energy Technology

Chalmers University of Technology

Abstract

Reducing CO_2 emissions is mandatory to mitigate climate change and carbon capture technologies are expected to play an important role in achieving the climate goals. Chemical-looping combustion (CLC) is promising due to its inherent separation of CO_2 together with efficient power and heat production. However, to maintain the cost-effectiveness of CLC there is a need for cheap and effective oxygen carriers. Calcium manganite is a highly reactive oxygen carrier, particularly suitable for high-volatile fuels such as biomass. This thesis investigates whether calcium manganite can form in-situ during CLC operation in a 300 W dual-fluidized bed reactor system using a natural manganese ore with CaO as an additive. The experiments were performed to evaluate the performance of the oxygen carrier, including reactivity towards syngas and methane, its oxygen uncoupling ability, as well as attrition at 950 °C. The results show that CaO addition together with prolonged fuel exposure improves reactivity towards methane and syngas as well as the formation of oxygen releasing phases. The highest methane conversion achieved was 85.2% at a fuel-reactor bed mass over fuel power of 780 kg/MW at 950 °C, exceeding the conversion achieved by the fresh ore. XRD analysis showed a phase evolution in the Mn-Ca mixture with the dominant phase changing from hausmannite to marokite, while SEM-EDX showed inter-particle transfer of Mn and Ca between particles after prolonged operation with more CaO addition. The findings show that addition of CaO to natural manganese ores can promote the in-situ formation of highly reactive oxygen carriers in a 300 W CLC reactor system while offering a route towards lower cost production of oxygen carriers for larger scale applications.

Keywords: Chemical-looping combustion (CLC), Chemical-looping with oxygen uncoupling (CLOU), Oxygen carrier, Fluidized bed reactor, In-situ formation, XRD, SEM-EDX

Acknowledgements

I would like to sincerely thank my supervisors Xiaoyun Li and Anders Lyngfelt for their guidance, valuable discussion and support throughout this work. A special thank you to Xiaoyun for her assistance with the operation of the reactor and always being quick to help when there were problems. I would also like to thank my examiner, Tobias Mattisson, for their constructive feedback and thoughtful evaluation. Thank you also to Niklas Engering and Henrik Leion for your insightful discussions during the meetings and thank you Niklas for casting my samples in epoxy for the SEM analysis.

This work was performed in part at the Chalmers Materials Analysis Laboratory, CMAL.

Acknowledgement of AI use

AI Software – ChatGPT and Claude has been used in this work to improve the language and grammar during the writing of the thesis.

Contents

1 Introduction 1
1.1 Climate change and CO_2 emissions 1
1.2 Carbon capture and storage 1
1.3 Chemical-looping combustion 2
1.4 Aim 3
2 Theory 4
2.1 Chemical looping combustion 4
2.2 Chemical-looping with oxygen uncoupling 5
2.3 Calcium manganite 6
3 Method and materials 8
3.1 Oxygen carrier 8
3.2 300 W reactor system 8
3.3 Experimental procedure 9
3.3.1 Overview of experimental conditions 10
3.3.2 Pure Eramet HM 11
3.3.3 CaO addition 11
3.3.4 Attrition 11
3.4 Characterization 12
3.5 Data evaluation 12
4 Results and discussion 14
4.1 Oxygen release from decomposition 14
4.2 CLOU effect 15
4.3 Reactivity towards CH_4 and syngas 16
4.3.1 Reactivity towards methane 16
4.3.2 Reactivity towards syngas 18
4.4 Attrition 19
4.5 Characterizations 20
4.5.1 XRD analysis 20
4.5.2 SEM-EDX 21
5 Conclusion 0

List of figures

Figure 1. Working principle of CLC. 4
Figure 2. 300 W CLC reactor....9
Figure 3. O_2 release from decomposition of Eramet HM during first warm-up of the ore. 14
Figure 4. Average O_2 release in FR during CLOU measurements at 950°C.....15
Figure 5. Comparison of reactivity at 950 °C of Eramet HM and lime mixture towards methane at different mixture ratios and operational hours where (a) is at the start of each day and (b) is at the end of each day after operation with syngas.....16
Figure 6. Conversion of syngas at varying fuel-reactor bed mass over fuel power from all the operational days. 18
Figure 7. SEM image and corresponding EDX elemental intensity maps for Mn and Ca of the cross-sections of Eramet HM & CaO mixture after operation with the first CaO addition. 22
Figure 8. SEM image and corresponding EDX elemental intensity maps for Mn and Ca of the cross-sections of Eramet HM & CaO mixture from day 6 of operation. 22
Figure 9. SEM image and corresponding EDX elemental intensity maps for Mn and Ca of the cross-sections of Eramet HM & CaO mixture from the last day of operation. 23
Figure 10. Points chosen for elemental analysis. 24
Figure 11. Elemental content at the core and surface layer of particles. 24

List of tables

Table 1. Elemental composition of manganese ore. 8
Table 2. Experimental conditions used for Eramet HM and Eramet HM & CaO in 300 W CLC reactor system.....10
Table 3. Attrition of Eramet HM and Eramet HM-Ca mixture in 300 W unit.....19
Table 4. Relative weight percentages of the different dominant phases observed, derived with semi-quantitative analysis of XRD data.....20

1 Introduction

1.1 Climate change and CO_2 emissions

The accumulation of greenhouse gases in the Earth's atmosphere is the main driver of ongoing climate change. The Intergovernmental Panel on Climate Change (IPCC) established that human activity has caused 1.1 °C of global warming relative to pre-industrial levels, with global temperatures projected to exceed 1.5 °C within the next two decades [1]. Carbon dioxide (CO_2) is the single largest contributor to the increase in global surface temperatures and according to the Emissions Database for Global Atmospheric Research (EDGAR), fossil CO_2 accounts for 74.5% of total global greenhouse gas emissions [2]. At the current CO_2 emission rate, the estimated carbon budget for having a 50% chance to limit global warming to 1.5°C will be exhausted before 2030 [3]. Achieving the climate targets of the Paris Agreement will therefore require immediate and deep reductions in emissions as well as the deployment of carbon capture and removal technologies [1].

1.2 Carbon capture and storage

Carbon capture and storage (CCS) is a mature technology that is deemed necessary to meet the goals of the Paris Agreement according to the IPCC. Several capture approaches have been developed, such as post-combustion capture, pre-combustion capture and oxy-fuel combustion. Among these, post-combustion capture using solvent-based absorption is the most mature technology. However, this technology suffers from energy-intensive gas separation and regeneration steps, leading to increased operational costs [4]. Similarly, oxy-fuel combustion suffers from requiring an air separation unit for oxygen production, which contributes to efficiency losses and increased costs [5].

Mitigation pathways proposed by the IPCC require the deployment of technologies capable of removing CO_2 from the atmosphere to fulfill the 1.5 °C target. One such approach is bioenergy with carbon capture and storage (BECCS), where CCS is combined with combustion of biomass to achieve negative emissions [6]. Biomass removes CO_2 from the atmosphere through photosynthesis, however, the same

amount removed is released during combustion. Therefore, the CO_2 released from combustion of biomass needs to be captured and permanently stored in geological formations such as saline aquifers or depleted oil fields in order to achieve negative emissions [7].

1.3 Chemical-looping combustion

Chemical looping combustion (CLC) is a technology that has inherent CO_2 separation, making it an attractive option compared to conventional CCS-technologies, since the expensive gas separation step can be avoided. CLC operates using two interconnected reactors, an air reactor (AR) and a fuel reactor (FR) [8]. In the AR, an oxygen carrier, a metal oxide, is oxidized using air before being transported to the FR where it is reduced while oxidizing the fuel by transferring lattice oxygen. This produces a stream consisting of CO_2 and H_2O and ideally a pure CO_2 stream is obtained after condensing the H_2O. CLC can be used with several different kinds of fuels, it has been proven to work with gaseous fuels and solid fuels such as biomass [9], making it viable for many kinds of operations. For solid fuel operation especially, it is important to have a cheap and effective oxygen carrier since material losses are higher because of the need to remove ash and attrition. During CLC with solid fuels, oxygen carriers that can release molecular oxygen in the FR, known as chemical-looping with oxygen uncoupling (CLOU), are preferred due to their higher reactivity and the avoidance of the slow fuel gasification step. Thus, performance is improved, which enables smaller reactor size and lower costs [10]. Calcium manganite is a CLOU material and has shown promising results when used as an oxygen carrier [11]. However, production of calcium manganite can be expensive. A recent study demonstrated that calcium manganite can form in-situ during CLC operation of manganese ores containing calcium [12]. In that work, the phase formation was observed for ores with inherently high Ca content and therefore the phase formation was assumed to occur within individual particles. In contrast, the present work aims to investigate whether any Mn-Ca phases can form through inter-particle transfer between initially separate manganese ore and CaO particles under CLC operating conditions. In this work, a natural manganese ore, Eramet HM, which has negligible inherent Ca content, is used. To investigate whether inter-particle transfer can lead to formation of Mn-Ca phases, Eramet HM was mixed with CaO and evaluated in a 300 W CLC-system.

1.4 Aim

The aim of the project is to investigate whether calcium manganite can form spontaneously during CLC operation through inter-particle transfer of Mn and Ca by mixing a natural manganese ore with CaO in a 300 W CLC reactor system. The purpose is to develop cheap and efficient oxygen carriers to be used in chemical looping combustion.

Specific questions to be answered:

1. How is the performance of mixtures of manganese ores with lime in a 300 W unit with respect to reactivity and attrition?
2. How do different parameters, such as the mixing ratio of manganese ore and lime, time of exposure to fuel gas affect the in-situ formation of calcium manganite?
3. Can any observed improvement in reactivity of the manganese ore in the 300 W system be correlated to the Ca-Mn phases by analyzing the samples through characterization tools, such as XRD and SEM-EDX.

2 Theory

2.1 Chemical looping combustion

Chemical looping combustion is an emerging technology that has inherent separation of CO_2. It operates with two interconnected fluidized bed reactors using an oxygen carrier to transfer oxygen from the air reactor (AR) to the fuel reactor (FR), see Figure 1. The AR is operated at a sufficiently high gas velocity to enable circulation of the oxygen carrier to the FR, whereas the FR is operated as a bubbling fluidized bed.

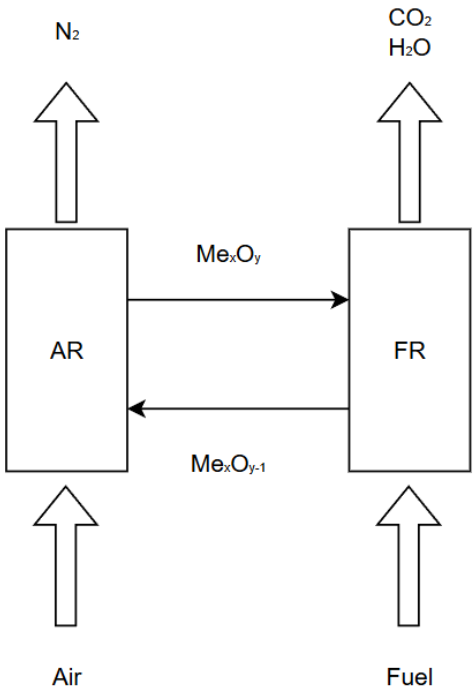

Figure 1. Working principle of CLC.

The oxygen carrier is oxidized by air in the AR according to reaction R1, where Me_xO_{y-1} denotes a metal oxide.

$$Me_xO_{y-1} + \frac{1}{2}O_2 \rightarrow Me_xO_y \qquad (R1)$$

The oxygen carrier is then transferred to the fuel reactor where it reacts with the fuel according to reaction R2, producing CO_2 and H_2O.

$$Me_xO_y + Fuel \rightarrow \ Me_xO_{y-1} + CO_2 + \ H_2O \qquad (R2)$$

After condensing the H_2O, a stream of almost pure CO_2 can be acquired. This allows for much cheaper separation compared to conventional post-combustion technologies due to the inherent gas separation [13].

2.2 Chemical-looping with oxygen uncoupling

Choosing the right oxygen carrier is essential for CLC and choosing an appropriate oxygen carrier depends on the application of CLC. Conversion of solid fuels in CLC is a complex process. First, the moisture of the fuel is evaporated, and the fuel then undergoes devolatilization, thus removing any volatile species. The remaining char is then gasified according to reactions R3 and R4 below.

$$C + H_2O \rightarrow CO + H_2 \quad (R3)$$

$$C + CO_2 \rightarrow 2CO \quad (R4)$$

Lastly, the products from the gasification can then be oxidized by the oxygen carrier, producing CO_2 and H_2O. The gasification is a slow process at the temperatures used in CLC, usually below 1000°C, leading to more expensive equipment due to larger size and longer residence times [14]. To bypass the slow gasification step, oxygen carriers that can release O_2 in the gas phase, called chemical-looping with oxygen uncoupling (CLOU), can be used. Three monometallic oxide systems have been investigated for the CLOU process namely, Mn_2O_3/Mn_3O_4, CuO/Cu_2O, and Co_3O_4/CoO [15]. These systems can release oxygen according to the following reactions.

$$4CuO \leftrightarrow 2Cu_2O + O_{2(g)} \quad (R5)$$

$$6Mn_2O_3 \leftrightarrow 4Mn_3O_4 + O_{2(g)} \quad (R6)$$

$$2Co_3O_4 \leftrightarrow 6CoO + O_{2(g)} \quad (R7)$$

However, copper-based oxides suffer from a relatively low melting point and tend to agglomerate, while the use of cobalt raises health and safety concerns. Both copper and cobalt are also more expensive compared to manganese. One problem with the

manganese oxide system is the relatively low temperature, around 800 °C, required for the re-oxidation to Mn_2O_3 in the AR. This problem can be solved by combining manganese with other elements to alter the properties of the oxygen carrier [16]. By combining with other elements, properties such as reactivity towards fuel or mechanical strength can be altered. The thermodynamics may also be altered by increasing the oxidation number of manganese, giving CLOU properties at relevant temperature.

2.3 Calcium manganite

Combining the manganese oxide system with other elements can be beneficial. One such system is the Mn-Ca system which is especially interesting since it can form calcium manganite ($CaMnO_{3-\delta}$), which has a perovskite structure. The perovskite structure can be written with the general formula $ABO_{3-\delta}$, where A and B are positively charged cations and A is typically the larger ion compared to B, the O corresponds to oxygen, which is the negatively charged ion in the structure[17]. The δ corresponds to the oxygen deficiency in the structure. The benefit of the perovskite structure is its ability to release oxygen without any changes to the crystal structure according to reaction R8. The oxygen deficiency can be increased or decreased by altering factors such as temperature or pressure, and the amount of gaseous oxygen available is expressed as $(\delta_{fr} - \delta_{ar})$.

$$\mathrm{CaMnO_{3-\delta ar}} \leftrightarrow \mathrm{CaMnO_{3-\delta fr}} + \frac{1}{2}(\delta_{fr} - \delta_{ar})O_2 \qquad (R8)$$

The thermodynamic properties of $CaMnO_{3-\delta}$ have previously been studied and it has been shown that it can release oxygen at the temperatures and pressures relevant to CLC [18]. Calcium manganite has been used as an oxygen carrier in previous studies where it has shown a high conversion of fuel, good CLOU properties and low attrition rates [19]. Calcium manganite can be produced synthetically. However, the production makes it more expensive and less attractive for larger scale operations. This makes it less attractive for applications using ash containing fuels such as coal and biomass due to the losses associated with ash removal [20]. Thus, it would be advantageous if

calcium manganite could be formed in a more cost-efficient way such as in-situ formation during the CLC operation when using natural manganese ores.

3 Method and materials

3.1 Oxygen carrier

The manganese ore Eramet HM was used as the base oxygen carrier and was evaluated in a 300 W chemical-looping combustion reactor system. The tests performed were CLOU effect, reactivity towards fuel and attrition. The elemental composition of the ore has previously been identified using ICP-SFMS (Inductively Coupled Plasma-Sector Field Mass Spectrometry) in another study [12] and can be seen in Table 1. The main crystalline phase in the fresh ore is MnO_2 (pyrolusite). The CaO was provided by Nordkalk AB and consists of 93 wt% CaO with minor amount of impurities such as SiO_2, MgO, Al_2O_3 and Fe_2O_3. Before operation the ores and the CaO were prepared by crushing and sieving to be within the range of 90 to 250 µm.

Table 1. Elemental composition of manganese ore.

Ore	Mn	Fe	Si	Al	Ti	Ca	K	Mg	Ba	Na	Total elements* (wt%)
Eramet HM (wt%)	53.6	7.1	1.7	4.5	0.1	0.1	1.1	0.1	0.4	0	68.7

*wt% missing to 100% is oxygen

3.2 300 W reactor system

The oxygen carrier was investigated in a 300 W reactor system consisting of two interconnected fluidized beds using two gaseous fuels, syngas and methane. The reactor used in the experiments is shown in Figure 2. The reactor is 300 mm high with a fuel reactor cross section of 25 × 25 mm and an air reactor cross section of 25 × 42 mm. In the upper section, the air reactor narrows down to a cross section of 25 × 25 mm thus raising the gas velocity to ensure that particles circulate from the AR to the FR.

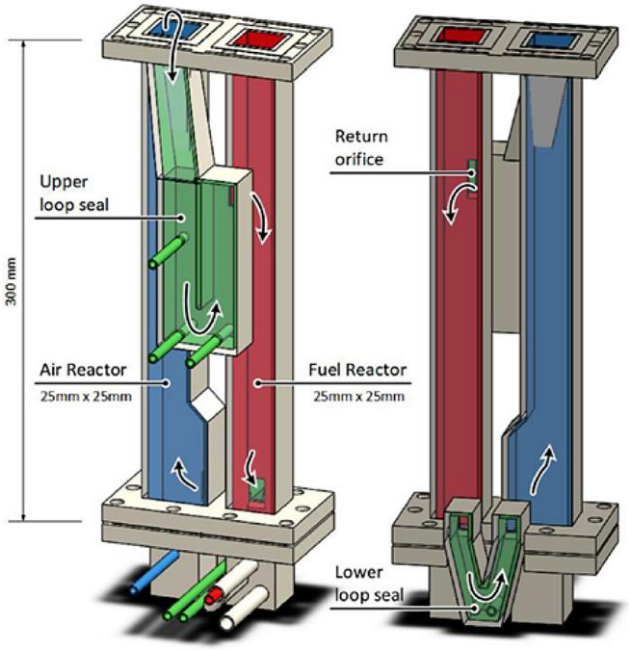

Figure 2. 300 W CLC reactor

Fuel and air enter the reactor from two separate wind boxes at the bottom of the reactor where porous quartz plates act as gas distributors. In the AR the flow of air drives the particles into the upper loop seal where the particles are then transported to the FR through the return orifice. The FR is operated as a bubbling fluidized bed and particles located at the bottom of the bed are transported back to the AR through the lower loop seal to begin a new cycle. Both of the loop seals are purged with an inert flow, usually argon or nitrogen, to ensure fluidization and that gases in both of the reactors are kept separated. A water seal connected to the FR outlet maintains a slightly higher pressure in the FR to prevent leakage from AR to FR. The temperature in the reactors beds is measured using thermocouples. Due to a high surface to volume ratio the reactor system is subject to high heat loss and to compensate for this and achieve the desired temperatures, the reactors are encased in a furnace. In this work the temperature used for every experiment is 950°C since solid diffusion is heavily dependent on temperature. The fluidization and circulation of particles are monitored through pressure sensors located at different heights in the two reactors.

3.3 Experimental procedure

The initial solids inventory of the oxygen carrier used was 400 g, which was poured from the chimney into the FR when the reactor was cold. When warming up the

reactor to the desired temperature, both the AR and FR were operated as bubbling fluidized beds with air flowing in both the AR and FR.
For the first warm-up, 1 L_n/min of inert N_2 was used as the fluidizing gas when warming up the reactor. This was done to account for the initial decomposition of MnO_2 occurring upon first heating of the ore.

3.3.1 Overview of experimental conditions

The CLOU effect was measured prior to each operation with fuel to monitor potential changes in oxygen release behavior. During these tests, the air flow is set to 8 L_n/min and the FR is fluidized with an inert gas, usually nitrogen or argon at 1 L_n/min. The pure Eramet HM was operated in the 300 W unit for one operational day, resulting in 3.3 hours with fuel. Following this day CaO was added directly to the solids inventory remaining in the reactor. The Eramet HM and CaO mixture was operated for 8 operational days, resulting in a total operating time with fuel of 49.6 hours.
For each operational day, except one, the reactivity towards methane was tested first, followed by a longer operation with syngas and lastly reactivity towards methane again. This was done to assess any changes in reactivity after operation with syngas. The basic settings used and operation time for each operational day can be seen in Table 2, here the variation in fuel flow is presented as the ratio of the FR bed mass over fuel power.

Table 2. Experimental conditions used for Eramet HM and Eramet HM & CaO in 300 W CLC reactor system.

Day	**CaO content (wt%)**	**AR flow ($L_n$min)**	**Temperature (°C)**	**CH_4 specific bed mass (kg/MW_{th})**	**Syngas specific bed mass (kg/MW_{th})**	**Fuel operation time (h)**
1	0	8	950	679 – 787	235 – 736	3.3
2	10	8	950	745 – 785	256 – 751	6.2
3	12.7	8	950	681 – 775	253 – 865	5.5
4	15.2	8	950	637 - 858	233 – 711	6.5
5	22.7	8	950	467 – 875	264 – 817	6.3

6	25	8	950	746 – 860	252 – 775	6.4
7	27.2	8	950	423 – 889	247 – 848	5.4
8	32.3	8	950	308 – 878	252 – 741	4.2
9	35.5	8	950	294 – 780	232 – 736	5.8

3.3.2 Pure Eramet HM

For the first operational day the performance of the pure manganese ore was tested to establish a reference for subsequent experiments involving CaO addition. The fuel flow was adjusted with the aim to achieve a FR bed mass over fuel power of 250 – 800 kg/MW_{th} for the syngas test and 800 kg/MW_{th} for the methane test.

3.3.3 CaO addition

After the operational day with pure Eramet HM, 34.1 g CaO was added to the reactor, corresponding to 10% of the weight of the remaining ore in the reactor after accounting for the loss on ignition and fines captured in the filters.

Following each operational day involving CaO addition, the reactor is cooled down in air and a 10 g sample was taken from the FR. To compensate for the removed sample, 10 g of CaO was added before the next day. Additional CaO was also added as make-up material when required to maintain the solids inventory between each operational day. In total 144.1 g of CaO was added.

3.3.4 Attrition

The fines captured in filters were collected and weighed after each day, in this work fines are defined as all the material that is captured in the filters. The attrition rate of the oxygen carriers was calculated as the mass of fines collected during operation divided by the initial solids inventory and the operating time with fuel according to Equation (1).

$$Attrition = \frac{m_{fines}}{m_{OC,initial} * t_{fuel}} * 100 \quad (1)$$

3.4 Characterization

The crystalline phases of the samples were analyzed using a BRUKER D8 Discovery with Cu radiation. Scanning electron microscopy with energy dispersive X-ray spectroscopy (Hitachi TM4000Plus Benchtop SEM) was used to analyze the chemical composition of the materials. The particles were prepared for SEM-EDX by casting the particles in epoxy and grinding the samples to obtain a cross-section.

3.5 Data evaluation

The reactors are connected to a gas sampling system to measure the O_2 concentration in both AR and FR as well as the concentration of the different carbon species found in the FR outlet. The conversion of fuel is assessed using the CO_2 yield seen in Equation (2). The CO_2 yield is the ratio of the volumetric concentration of CO_2 to the carbon species found in the outlet gas of the FR.

$$CO_2\ yield = \frac{CO_2}{CO_2 + CO + CH_4} \tag{2}$$

Due to the circulation of oxygen carrier between the two reactors, the bed inventory in each reactor may vary during operation. The amount of oxygen carrier present in the fuel reactor strongly influences the fuel conversion and therefore it is important to know the specific bed mass in the reactors when evaluating the conversion. To estimate the bed inventory in each reactor, Equation (3) and (4) can be used

$$m_{bed,FR} = \frac{\Delta P_{FR} * A_{FR}}{g} \tag{3}$$

$$m_{bed,AR} = \frac{\Delta P_{AR} * A_{AR}}{g} \tag{4}$$

Where ΔP is the pressure drop over the reactor, A is the cross-sectional area and g is the acceleration of gravity. When evaluating the performance of the oxygen carrier, the ratio between FR bed mass, $m_{bed,FR}$, and fuel power is often used and is usually expressed in kg/MW_{th}. The ratio between FR bed mass and fuel power represents the amount of oxygen carrier available per unit of fuel input. This ratio is useful since it allows the result obtained in smaller reactors to be compared with larger reactors as well as enabling comparison when using different solids inventory or oxygen carriers. Thus, for a reactor with fixed cross-sectional area and FR pressure drop measurement the fuel flow required to achieve a certain specific FR bed mass can be estimated.

4 Results and discussion

4.1 Oxygen release from decomposition

During the first heat-up of the ore, both AR and FR were operated as described in section 3.3.1, with nitrogen flowing through both reactors since a large amount of O_2 is released due to the decomposition of MnO_2. The oxygen released can be seen in Figure 3. The release began at approximately 410 °C and reached a maximum at around 600°C, where the O_2 concentration exceeded the measurement limit of the gas analyzer (25.25 vol%). This release corresponds to the decomposition of MnO_2, which is the main phase in the fresh ore, to Mn_2O_3. After reaching 600 °C the O_2 concentration stabilized around 1.9% in both the AR and FR until the reactors reached around 880°C where another decomposition reaction happened. The second oxygen release is explained by the decomposition of Mn_2O_3 to Mn_3O_4. Once the decomposition had been completed, the reactors were heated to 950 °C, the initial heat-up took approximately 130 minutes.

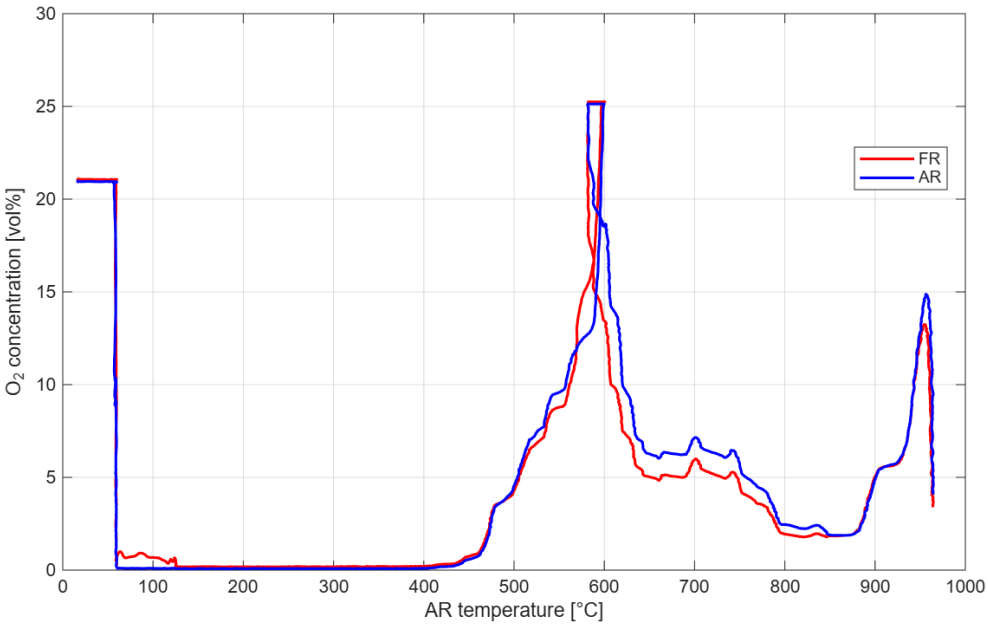

Figure 3. O_2 release from decomposition of Eramet HM during first warm-up of the ore.

4.2 CLOU effect

The CLOU effect was measured both before and after fuel operation during each operational day and the average O_2 release in the FR can be seen in Figure 4.

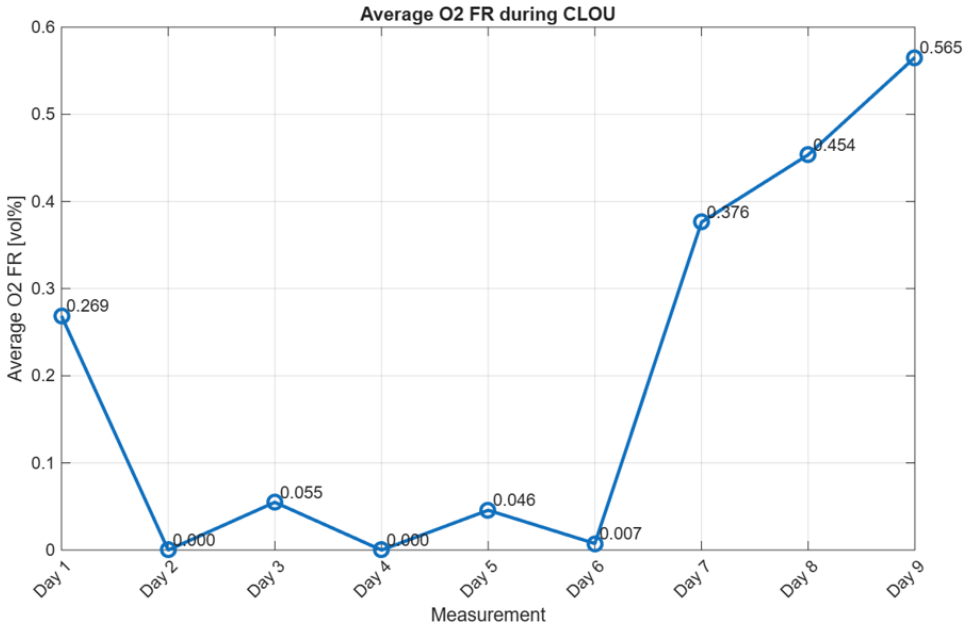

Figure 4. Average O_2 release in FR during CLOU measurements at 950°C.

On day 1 with the pure Eramet HM ore the average O_2 released was 0.27 vol% and for day 2 - 6 where the amount of CaO added was between 10 – 25 wt% the oxygen release was either negligible or zero. The reason for the observed CLOU effect on day 1 and not for the following days could be the presence of Mn_2O_3 in the particles due to incomplete decomposition. During the CLOU test at day 7, after 39 hours of operation, a significant increase in the O_2 release was seen, reaching an average concentration of 0.38 vol% in the FR. For the next two operational days, the average O_2 release of the mixture during the CLOU tests increased to 0.45 vol% and 0.57 vol% respectively. This suggests that prolonged fuel exposure together with an adequate mixture of manganese ore and lime promotes the formation of oxygen releasing phases.

4.3 Reactivity towards CH_4 and syngas

4.3.1 Reactivity towards methane

The reactivity of Eramet HM was investigated under increasing addition of CaO and increasing number of operational hours, as well as at different fuel flows. The different fuel flows are presented as the ratio between the mass of the oxygen carrier and CaO particles in the fuel reactor and the thermal power of the fuel. Methane conversion at different operating times and CaO contents is shown in Figure 5. Figure 5(a) shows methane conversion at the start of each day, prior to syngas exposure, while Figure 5(b) shows methane conversion after operation with syngas. At the start of the day with 12.6 wt% of CaO, no reactivity test with methane was performed. Thus, only values for the reactivity at the end of this day are available.

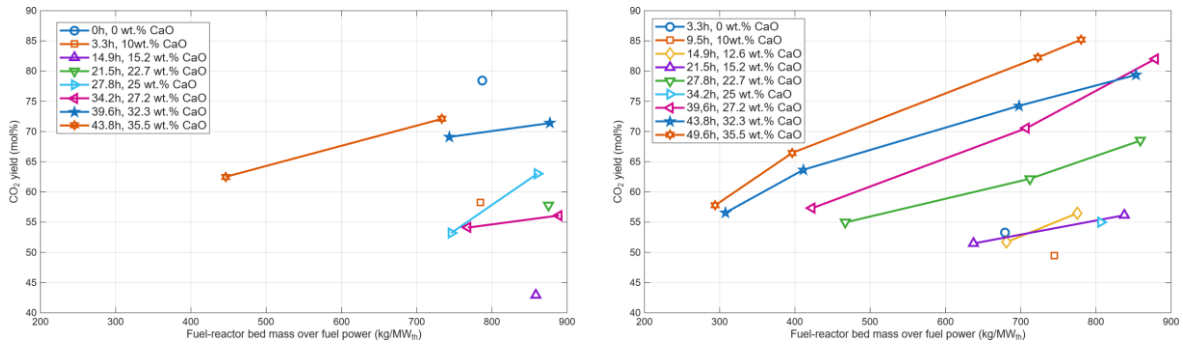

(a) (b)

Figure 5. Comparison of reactivity at 950 °C of Eramet HM and lime mixture towards methane at different mixture ratios and operational hours where (a) is at the start of each day and (b) is at the end of each day after operation with syngas.

For the very first operational day where pure Eramet HM was used the methane conversion at the start was 79% at a fuel-reactor bed mass over fuel power of 787 kg/MW represented by the blue circle in Figure 5 (a). By the end of this operational day the methane conversion had decreased. At a fuel-reactor bed mass over fuel power of 679 kg/MW, the methane conversion was 53% represented by the blue circle in Figure 5 (b). A lower conversion is expected since the FR bed mass over fuel power is lower, however the decrease is too large to only be explained by this. One explanation could

be a higher content of Mn_2O_3 present in the particles at the start of the day, which undergoes decomposition to Mn_3O_4 during the syngas operation.

For the second day when 10 wt% of CaO has been added, represented by the orange square in Figure 5 (a) and (b), a similar trend is seen where the methane conversion is lower after the longer operation with syngas. However, beyond this point the trend changes. For all the other operational days there is a clear increase in methane conversion after operation with syngas suggesting that exposure to syngas can increase the reactivity of Eramet Hm Mn ore with lime added. One exception to this is day 6 with 25 wt% CaO which saw a decrease in the conversion.

Notably, the highest increase in methane conversion from 55% at 806 kg/MW with 25 wt% CaO to 82% at 878 kg/MW with 27.2 wt% CaO coincides with the observed increase in O_2 release during the CLOU tests on day 7. This suggests that the increase in conversion could be related to the formation of oxygen releasing phases. The highest methane conversion was observed on the last day after 49.6 h of fuel operation, reaching 85.2% at a specific FR bed mass over fuel power of 780 kg/MW, represented by the orange lines in Figure 5 (a) and (b). Compared to the initial conversion of methane with the fresh ore, this represents a substantial improvement in the reactivity towards methane.

4.3.2 Reactivity towards syngas

The results from the reactivity test towards syngas can be seen in Figure 6. Initially, the conversion of syngas decreased with decreasing FR bed mass over fuel power represented by the blue line in Figure 6.

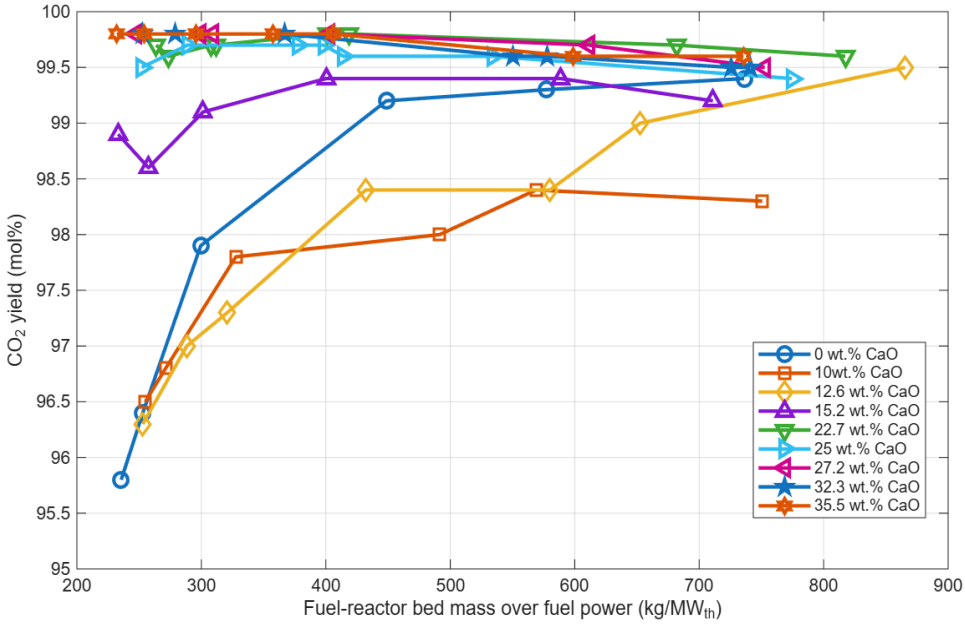

Figure 6. Conversion of syngas at varying fuel-reactor bed mass over fuel power from all the operational days.

For the first two operational days with CaO addition, the syngas conversion was lower than without CaO. This is likely explained by the removal of oxygen carrier material and its replacement with CaO, resulting in a less reactive oxygen carrier material.

For the operational day with 15.2 wt% CaO, the syngas conversion improved and exceeded the conversion achieved by the pure ore. The inventory of Eramet HM oxygen carrier material was lower for this operation compared to earlier days, indicating that the addition of CaO can improve the reactivity.

This increase in conversion is consistent with the methane reactivity results, as the first increase in methane conversion was observed during the same day. Syngas conversion also followed a similar trend to the methane conversion, where conversion increased during subsequent days, except for the day containing 25 wt% CaO.

4.4 Attrition

The amount of fines collected each day, as well as the attrition rate, can be seen in Table 3, where day 1 is for the pure manganese ore and the subsequent days are for the mixture.

Table 3. Attrition of Eramet HM and Eramet HM-Ca mixture in 300 W unit

Day	**CaO added (g)**	**Collected fines (g)**	**Fuel operation time (h)**	**Attrition rate (wt%/h)**
1	0	2.5	3.3	0.19
2	34.1	3.3	6.2	0.13
3	10	4.5	5.5	0.20
4	10	12.9	6.5	0.50
5	30	10.8	6.3	0.43
6	10	3.2	6.4	0.13
7	10	6.3	5.4	0.29
8	24	6.7	4.2	0.40
9	16	5.1	5.8	0.22
Total/Average		58.9	49.6	0.28

The attrition rate for the Mn-Ca mixture was higher than what has previously been reported for pure Eramet HM which was 0.07 wt%/h [12]. A possible explanation for this is that CaO may have poor integrity, thus turning into fines. Days 5 and 8 had a larger amount of make-up CaO added before operation and these days show a higher attrition rate suggesting poor integrity of CaO. During operation on day 4 it was observed that fines had accumulated in the outlet pipes due to insufficient cleaning after each operation. This issue was solved during operation and is probably the reason why day 4 saw an increase in collected fines. The fines collected that day are most likely a mixture of fines from the previous operations together with fines formed during day 4.

4.5 Characterizations

4.5.1 XRD analysis

The evolution of the major crystalline phases, in terms of semi-quantitative wt%, observed in the collected samples from each day, is shown in Table 4.

Table 4. Relative weight percentages of the different dominant phases observed, derived with semi-quantitative analysis of XRD data.

Day	**Cumulative operational hours**	**CaO (wt%)**	**Hausmannite $(Mn,Fe)_3O_4$ (wt%)**	**Marokite $CaMn_2O_4$ (wt%)**
1	3.3	0	100	0
2	9.5	65	35	0
3	14.9	40	60	0
4	21.5	16	68	16
5	27.8	44	33	23
6	34.2	62	20	18
7	39.6	62	12	23
8	43.8	61	0	39
9	49.6	71	0	29

The dominant phase observed in the pure manganese ore after operation in the 300 W unit was hausmannite, while none of the phases presented for the fresh ore in Table 2 could be identified. Following the first addition of CaO on day 2, sharp CaO peaks were observed, and the dominant manganese phase remained unchanged. The semi-quantitative analysis estimated the CaO content to be 65 wt%, which is substantially higher than the amount added (10 wt%). This is most likely due to the high intensity of the CaO peaks combined with noise from the manganese ore phases caused by the Cu radiation used. Nevertheless, the semi-quantitative analysis can still provide useful insights into the evolution of the dominant phases throughout the different days.

There was no significant phase evolution observed between day 2 and 3. However, on day 4, the phase $CaMn_2O_4$ (marokite) was first observed. The appearance of marokite and the lower wt% of CaO suggests that interactions between Ca and Mn may have begun to occur. The smaller amount of CaO observed this day with XRD could also be explained by the larger amount of fines formed this day. Day 4 was also the first day that an increase in the reactivity towards both fuels used was seen, suggesting that the presence of marokite may have contributed to this behavior. However, marokite has not been studied as an oxygen carrier and its properties as an oxygen carrier remain largely unknown. A possible explanation for the increased reactivity is that a small amount of $CaMnO_3$ is formed on the surface of the particles, albeit undetectable with XRD, as XRD is a bulk measurement technology.

During the following days a significant shift in dominant phases was observed and the semi-quantitative wt% of marokite gradually increased each day, eventually becoming the dominant Mn-phase on day 7 after 39.6 h of operation. Notably, day 7 was also the first day that the CLOU effect was seen, see Figure 4. The last two days of operation saw an increase in the marokite phase, while the hausmannite phase disappeared. This increase in marokite coincides with an increase in oxygen released as well as an increase in reactivity.

4.5.2 SEM-EDX

The samples collected were further investigated through SEM-EDX to characterize the spatial distribution of Mn and Ca within the particles. Samples taken after day 2, 6 and 9 were analyzed. Figure 7 shows the elemental distribution for the sample taken after day 2 with 10 wt% CaO added. The Eramet HM-CaO mixture appeared to consist primarily of separate manganese ore particles and CaO particles, suggesting that limited interaction between the two materials had occurred at this stage.

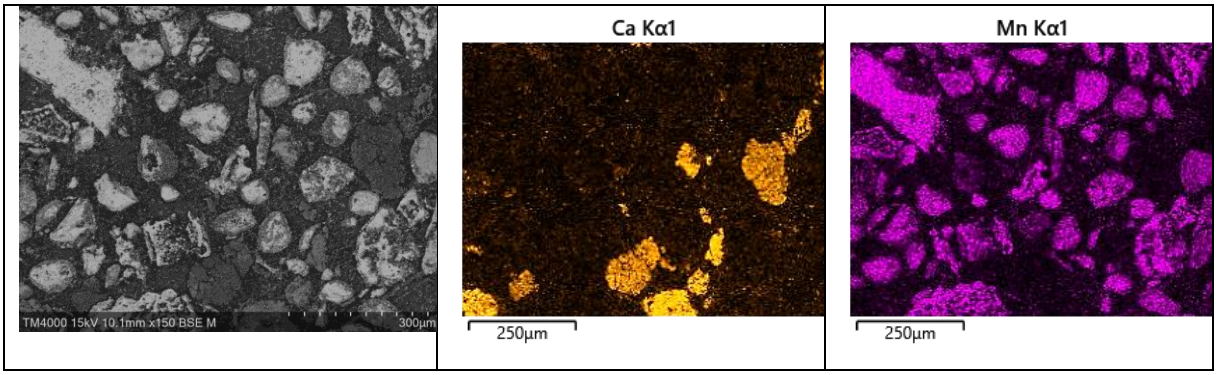

Figure 7. SEM image and corresponding EDX elemental intensity maps for Mn and Ca of the cross-sections of Eramet HM & CaO mixture after operation with the first CaO addition.

The elemental mapping of the sample taken after day 6 with 25 wt% CaO can be seen in Figure 8. Compared to the samples taken after day 2, a distinct surface layer of Ca particles could now be observed on the Mn ore particles, suggesting that inter-particle transfer of Mn and Ca had occurred at this stage. There is also a small surface layer of Mn seen on the CaO particles suggesting that the transfer occurred in both directions. These observations coupled with the increasing amount of marokite seen with XRD could be an explanation of the increase in reactivity towards methane and syngas through the formation of Mn-Ca phases.

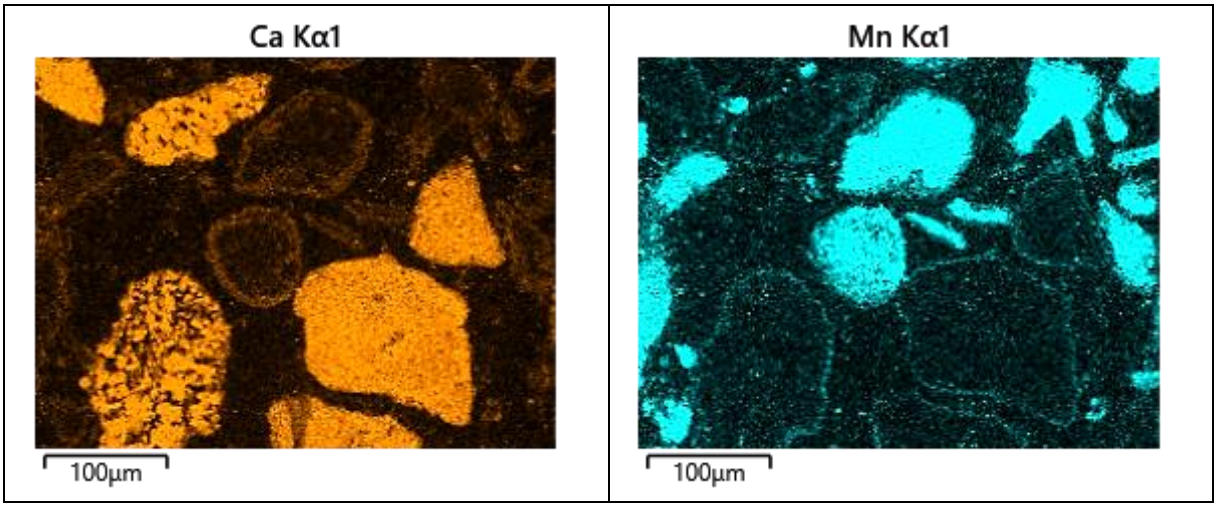

Figure 8. SEM image and corresponding EDX elemental intensity maps for Mn and Ca of the cross-sections of Eramet HM & CaO mixture from day 6 of operation.

Figure 9 shows the elemental mapping for the sample taken after the last operation on day 9. In contrast to the sample collected on day 2 and day 6, Ca could now be observed deeper within the Mn-rich particles suggesting Ca can become incorporated into the Mn ore after prolonged operation. In addition to this, a Mn-rich surface layer, albeit thinner, can be seen on the Ca-rich particles. This indicates that the transfer of

Mn to Ca-rich particles is slower than the transfer of Ca to Mn-rich particles. However, fresh CaO is added before each operation. Thus, the observed Ca particle could be a newly added particle.

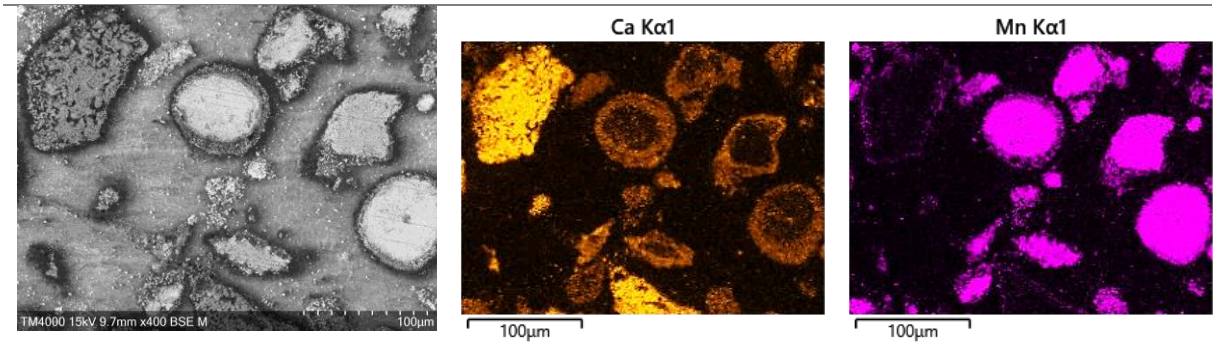

Figure 9. SEM image and corresponding EDX elemental intensity maps for Mn and Ca of the cross-sections of Eramet HM & CaO mixture from the last day of operation.

Point analysis was conducted on the core and surface of certain particles in the final sample to evaluate their elemental composition. The selected analysis points can be seen in Figure 9, while Figure 10 presents the mol% of each element identified in each point. Several surface layer points showed relatively similar Mn and Ca content, whereas others were either Mn-rich or Ca-rich. It can also be seen that the core of Mn-rich and Ca-rich particles, such as those represented by points S2, S8 and S9 contained mostly Mn or Ca. This indicates that the transfer of elements has not reached the center of the particles. Points S3 and S4 exhibited Mn:Ca ratios close to 1, which could indicate the formation of $CaMnO_3$. This would agree with the observation of the CLOU effect. However, it is reasonable to assume that any extent of $CaMnO_3$ formation is limited to the surface of the particles. Since this phase could not be detected through the XRD measurements and the 1:1 molar ratio of Mn and Ca could only be detected in the surface layer.

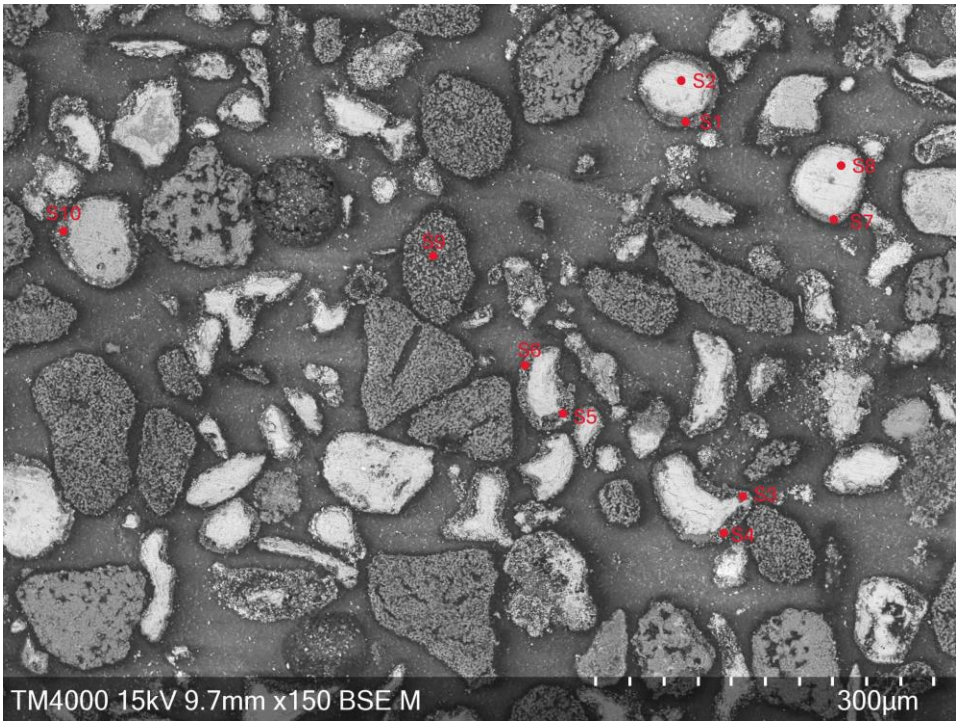

Figure 10. Points chosen for elemental analysis.

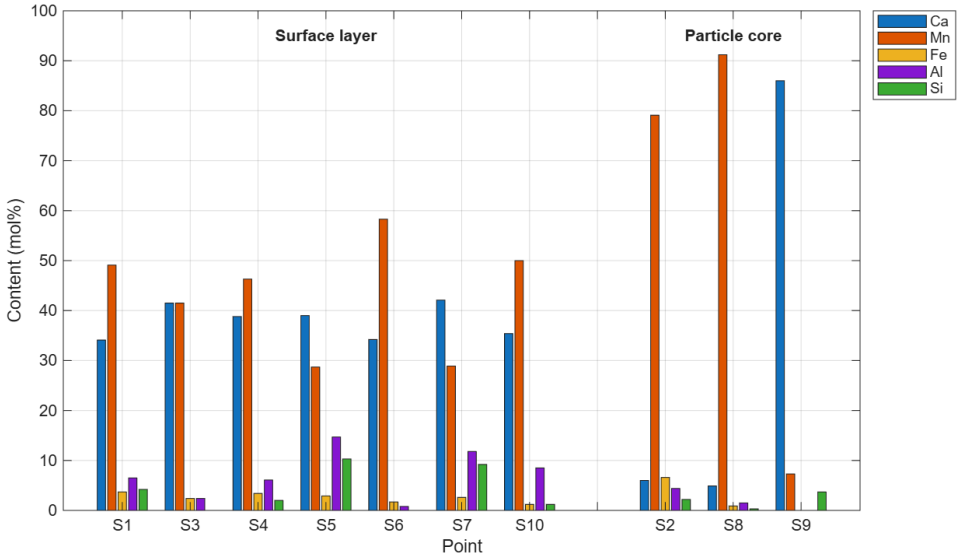

Figure 11. Elemental content at the core and surface layer of particles.

For the point analysis done on the final sample only point S6 exhibited a Mn:Ca close to the ratio for marokite which is 2:1 while the other points were close to a ratio of 1:1. Since the dominant phase observed with XRD was marokite this could indicate that the marokite phase exists beyond the surface layer. Nevertheless, the characterization observations show that the Mn-Ca phases formed could be the cause of the increase

in the performance of the Mn ore. Although it is still uncertain what is causing this increase in performance, in previous work marokite has been seen as an unwanted byproduct of $CaMnO_3$. With marokite being the dominant phase observed for this mixture, it could indicate that marokite might be the active phase causing the observed increase in performance. A recent study showed that marokite could have oxygen deficiency, much like $CaMnO_3$ which further could support the idea that marokite might be the active phase in this mixture [21].

5 Conclusion

This work investigated the performance of a mixture of the manganese ore, Eramet HM, and lime as well as in-situ formation of calcium manganite during chemical-looping combustion in a 300 W CLC reactor system.

The results showed that prolonged operation with increasing CaO addition improved both methane and syngas conversion. On day 7 of operation, the Mn-Ca mixture exhibited the CLOU effect indicating that CaO addition to manganese ores promoted the formation of oxygen-releasing phases.

XRD analysis showed a significant evolution of phases during the operation. The dominant phase shifted from hausmannite $(Mn,Fe)_3O_4$ to marokite ($CaMn_2O_4$), indicating incorporation of Ca into the Mn-phases. SEM-EDX further supported this by showing significant inter-particle transfer between Mn-rich and Ca-rich particles with a mixture containing 35.5 wt% CaO after 49.6 h of operation. Point analysis on certain particles showed a Mn:Ca molar ratio of close to 1:1 on the surface of these particles, suggesting formation of $CaMnO_3$. However, the dominant phase identified by XRD was marokite while $CaMnO_3$ could not be detected.

The increase in reactivity towards syngas and methane coincided with the formation of the Mn-Ca phases observed with characterization tools, suggesting these phases contributed to the improved oxygen carrier performance. Although marokite was the dominant phase, the observed CLOU effect indicates that oxygen releasing phases were also present but remained below the detection limit of XRD measurements. This suggests that either $CaMnO_3$ is formed but not detected, or that marokite may be able to release oxygen.

References

[1] K. Calvin *et al.*, "IPCC, 2023: Climate Change 2023: Synthesis Report. Contribution of Working Groups I, II and III to the Sixth Assessment Report of the Intergovernmental Panel on Climate Change [Core Writing Team, H. Lee and J. Romero (eds.)]. IPCC, Geneva, Switzerland.," Intergovernmental Panel on Climate Change (IPCC), Jul. 2023. doi: 10.59327/IPCC/AR6-9789291691647.

[2] European Commission. Joint Research Centre., *GHG emissions of all world countries: 2025.* LU: Publications Office, 2025. Accessed: May 01, 2026. [Online]. Available: https://data.europa.eu/doi/10.2760/9816914

[3] P. Friedlingstein *et al.*, "Global Carbon Budget 2025", Accessed: May 01, 2026. [Online]. Available: https://essd.copernicus.org/preprints/essd-2025-659/

[4] J. Du *et al.*, "Review on post-combustion CO2 capture by amine blended solvents and aqueous ammonia," *Chemical Engineering Journal*, vol. 488, p. 150954, May 2024, doi: 10.1016/j.cej.2024.150954.

[5] C. Ekström *et al.*, "Techno-Economic Evaluations and Benchmarking of Pre-combustion CO2 Capture and Oxy-fuel Processes Developed in the European ENCAP Project," *Energy Procedia*, vol. 1, no. 1, pp. 4233–4240, Feb. 2009, doi: 10.1016/j.egypro.2009.02.234.

[6] M. Rydén *et al.*, "Negative CO2 Emissions with Chemical-Looping Combustion of Biomass – A Nordic Energy Research Flagship Project," *Energy Procedia*, vol. 114, pp. 6074–6082, Jul. 2017, doi: 10.1016/j.egypro.2017.03.1744.

[7] J. Kemper, "Biomass and carbon dioxide capture and storage: A review," *International Journal of Greenhouse Gas Control*, vol. 40, pp. 401–430, Sep. 2015, doi: 10.1016/j.ijggc.2015.06.012.

[8] "Chemical Looping Combustion - an overview | ScienceDirect Topics." Accessed: Jan. 30, 2026. [Online]. Available: https://www.sciencedirect.com/topics/engineering/chemical-looping-combustion

[9] A. Lyngfelt, "Chemical Looping Combustion: Status and Development Challenges," *Energy Fuels*, vol. 34, no. 8, pp. 9077–9093, Aug. 2020, doi: 10.1021/acs.energyfuels.0c01454.

[10] H. Leion, T. Mattisson, and A. Lyngfelt, "Using chemical-looping with oxygen uncoupling (CLOU) for combustion of six different solid fuels," *Energy Procedia*, vol. 1, no. 1, pp. 447–453, Feb. 2009, doi: 10.1016/j.egypro.2009.01.060.

[11] M. Källén, M. Rydén, C. Dueso, T. Mattisson, and A. Lyngfelt, "CaMn0.9Mg0.1O3-δ as Oxygen Carrier in a Gas-Fired 10 kWthChemical-Looping Combustion Unit," *Ind. Eng. Chem. Res.*, vol. 52, no. 21, pp. 6923–6932, May 2013, doi: 10.1021/ie303070h.

[12] X. Li, R. Faust, A. Lyngfelt, P. Knutsson, and T. Mattisson, "Noncalcined Manganese Ores as Oxygen Carriers for Chemical Looping Combustion with Oxygen Uncoupling in a Circulating Fluidized Bed Reactor System," *Energy Fuels*, vol. 38, no. 17, pp. 16657–16677, Sep. 2024, doi: 10.1021/acs.energyfuels.4c02406.

[13] A. Lyngfelt and B. Leckner, "A 1000 MWth boiler for chemical-looping combustion of solid fuels – Discussion of design and costs," *Applied Energy*, vol. 157, pp. 475–487, Nov. 2015, doi: 10.1016/j.apenergy.2015.04.057.

[14] H. Leion, T. Mattisson, and A. Lyngfelt, "The use of petroleum coke as fuel in chemical-looping combustion," *Fuel*, vol. 86, no. 12, pp. 1947–1958, Aug. 2007, doi: 10.1016/j.fuel.2006.11.037.

[15] T. Mattisson, A. Lyngfelt, and H. Leion, "Chemical-looping with oxygen uncoupling for combustion of solid fuels," *International Journal of Greenhouse Gas Control*, vol. 3, no. 1, pp. 11–19, Jan. 2009, doi: 10.1016/j.ijggc.2008.06.002.
[16] M. Rydén, H. Leion, T. Mattisson, and A. Lyngfelt, "Combined oxides as oxygen-carrier material for chemical-looping with oxygen uncoupling," *Applied Energy*, vol. 113, pp. 1924–1932, Jan. 2014, doi: 10.1016/j.apenergy.2013.06.016.
[17] K. Wang, C. Han, Z. Shao, J. Qiu, S. Wang, and S. Liu, "Perovskite Oxide Catalysts for Advanced Oxidation Reactions," *Advanced Functional Materials*, vol. 31, no. 30, p. 2102089, 2021, doi: 10.1002/adfm.202102089.
[18] E. Bakken, T. Norby, and S. Stølen, "Nonstoichiometry and reductive decomposition of CaMnO3−δ," *Solid State Ionics*, vol. 176, no. 1, pp. 217–223, Jan. 2005, doi: 10.1016/j.ssi.2004.07.001.
[19] X. Li *et al.*, "Performance of a perovskite-structured calcium manganite oxygen carrier produced from natural ores in a batch reactor and in operation of a chemical-looping combustion reactor system," *Chemical Engineering Journal*, vol. 497, p. 154516, Oct. 2024, doi: 10.1016/j.cej.2024.154516.
[20] I. Gogolev *et al.*, "Chemical-looping combustion in a 100 kW unit using a mixture of synthetic and natural oxygen carriers – Operational results and fate of biomass fuel alkali," *International Journal of Greenhouse Gas Control*, vol. 88, pp. 371–382, Sep. 2019, doi: 10.1016/j.ijggc.2019.06.020.
[21] S. Ma, J. Min, Y. Zhou, T. Yang, X. Zhao, and K. Shih, "Beyond CaMnO3-δ: Unlocking Cation and Oxygen Vacancies and Potential Thermal Energy Storage in Ca(1-x)Mn2O4-δ," *Materials Today Energy*, vol. 53, p. 102040, Oct. 2025, doi: 10.1016/j.mtener.2025.102040.